Advanced Composite Materials
Publication details, including instructions for authors and subscription information:
http://www.tandfonline.com/loi/tacm20

Analysis of transverse cracking in cross-ply composite laminates

F.S. Ji [a] , L.R. Dharani [b] & S. Mall [c]

[a] Department of Mechanical and Aerospace Engineering and Engineering Mechanics, University of Missouri-Rolla, Rolla, MO 65409-0050, USA

[b] Department of Mechanical and Aerospace Engineering and Engineering Mechanics, University of Missouri-Rolla, Rolla, MO 65409-0050, USA

[c] Department of Aeronautics, Air Force Institute of Technology, Wright Patterson Air Force Base, OH 45433, USA

Version of record first published: 02 Apr 2012.

To cite this article: F.S. Ji , L.R. Dharani & S. Mall (1998): Analysis of transverse cracking in cross-ply composite laminates, Advanced Composite Materials, 7:1, 83-103

To link to this article: http://dx.doi.org/10.1163/156855198X00075

Adv. Composite Mater., Vol. 7, No. 1, pp. 83–103 (1998)

Analysis of transverse cracking in cross-ply composite laminates

F. S. JI,[1] L. R. DHARANI[1,*] and S. MALL[2]

[1]*Department of Mechanical and Aerospace Engineering and Engineering Mechanics, University of Missouri-Rolla, Rolla, MO 65409-0050, USA*

[2]*Department of Aeronautics, Air Force Institute of Technology, Wright Patterson Air Force Base, OH 45433, USA*

Received 1 November 1996; accepted 9 September 1997

Abstract—An analytical model based on the principle of minimum potential energy is developed and applied to determine the two-dimensional thermoelastic stress state in cross-ply composite laminates containing multiple equally spaced transverse cracks in the 90° plies and subjected to tensile loading in the longitudinal direction. The model provides full field solution for displacements and stresses including the residual thermal stresses which in turn are used to calculate the strain energy release rate associated with various failure modes. The strain energy release rate criterion has been employed to evaluate the critical applied stresses for two of the possible fracture modes; self-similar extension of a pre-existing flaw and the formation of a new parallel crack. The computed results indicate that formation of new cracks never takes place until pre-existing cracks extend through the entire thickness of the 90° plies. The predicted results of transverse crack density are in good agreement with the available experimental data.

Keywords: Transverse cracking; stiffness; energy release rate; cross-ply laminates; critical stress; crack density.

1. INTRODUCTION

In most continuous fiber cross-ply composite laminates, transverse matrix cracking or microcracking takes place in the 90° plies at strain levels which are very small compared to the ultimate failure strain of the laminate. In general, these transverse matrix cracks are equally spaced in the longitudinal direction. This phenomenon has been observed in polymer matrix composites by Garrett and Bailey [1], Parvizi *et al* [2], Bailey *et al.* [3], Highsmith and Reifsnider [4], Crossman and Wang [5], Wang *et al.* [6], Wang [7], Ogin *et al.* [8], Smith and Wood [9], and Liu and Nairn [10]. They have found that transverse matrix cracking typically starts at low strain levels in the weakest 90° plies and manifests in continual drop in the laminate stiffness with either

*To whom correspondence should be addressed, E-mail: dharani@umr.edu

increased or repeated loading. Dvorak and Johnson [11] have observed that in metal matrix composite laminates, matrix cracking appears to be caused only by cyclic loads which exceed the shakedown limit of the laminate. The crack patterns and densities are generally similar to those found in polymer matrix systems. Transverse matrix cracking in ceramic matrix composites has been observed by Seerat-un-Nabi and Derby [12], Pryce and Smith [13] and Mall and Bachmann [14]. Although the formation of transverse cracks does not precipitate into catastrophic failure, their presence can be very undesirable. They may not only cause a decrease in laminate stiffnesses [4, 15–22], but also alter the thermal properties [23–25]. The stiffness-reduction and the change in thermal expansion coefficients have been related to the density of transverse cracks in the 90° plies.

It is well known that the transverse crack density depends on the applied load, the configuration and mechanical properties of composite laminates. The growth of transverse cracks in composite laminates can be looked upon as an accumulation of many fracture events and can be characterized by relating the applied load to the density of transverse crack (number of cracks per unit length). Several analytical approaches involving a stress analysis scheme and an approximate failure criterion have been reported to analyze the transverse cracking problem. Garrett and Bailey [1] used the shear-lag assumption to analyze the stress state of damaged laminates and used the first ply failure criterion to predict the propagation of a transverse crack. Flaggs [26] also used the classical shear-lag assumption for the analysis of stress field and used the strain energy release rate for fracture analysis. Wang *et al.* [27] presented their simulation model for the growth of multiple transverse cracks subjected to both static and fatigue loads by introducing statistical distributions for effective flaw size and location in the 90° plies. Laws and Dvorak [28] investigated progressive cracking based on statistical fracture mechanics, in which the classical shear-lag theory was used to calculate the stresses and the strain energy release rate for failure and an empirical probability density function for the location of new cracks. Nairn [25] gave an explicit formulation by using the variation approach proposed by Hashin [17] to calculate the thermoelastic stress state and the strain energy release rate criterion to relate the applied load to the crack density. Liu and Nairn [10] corrected a mistake on the explicit formulation of Nairn [25], and further improved formulation by introducing a correction factor of crack spacing. They also conducted experimental work to validate their model, in which they matched the predicted results with the experimental data by varying the fracture toughness and the correction factor of crack spacing. Han and Hahn [20] developed a model to characterize multiple transverse cracks, using a resistance curve based on the concept of a through-the-thickness inherent flaw and energy balance principle. Zhang *et al.* [29] used the improved two-dimensional shear-lag analysis to calculate the stress distributions in the damaged laminates and the corresponding strain energy release rate due to transverse cracking and predicted crack growth with increasing applied load by employing the resistance curve concept. As opposed to the above models, Guild *et al.* [30] developed a three-dimensional finite element model to investigate the growth of transverse cracks in the width direction of cross-ply composite laminates, based on the concept of strain energy release rate.

In all the previous research work except that of Guild *et al.* [30] on the fracture analysis of transverse cracking, multiple transverse cracks are assumed to span the entire thickness of the 90° plies and the entire width of laminates. The accumulation of damage is essentially due to multiple transverse cracks only. The problem in which the transverse cracks only partly span the thickness of the 90° plies has not been addressed in the previous studies. In this paper, an analytical model based on the principle of minimum potential energy [31] is developed and applied to study the stress field in a laminate containing an inherent flaw within 90° ply group. The computed stress field is used to calculate the strain energy release rates associated with two fracture modes; formation of a new crack and the extension of a pre-existing crack. The analysis includes the effect of residual thermal stress. The strain energy release rate criterion has been employed to evaluate the critical applied stresses for the two fracture modes and competition between formation of a new crack and the growth of a pre-existing crack. Finally, the parametric studies on transverse cracking problem are done for two systems of composite materials, $[0_3^\circ/90^\circ]_s$ ceramic/ceramic (SiC/1723) and $[0^\circ/90_3^\circ]_s$ glass/epoxy laminates and analytical results are compared with the available experimental data.

2. FORMULATION

A schematic edge view of a composite laminate considered in this analysis is shown in Fig. 1. The laminate consists of 0° plies and 90° plies. Each of the 0° and 90° ply groups is assumed to be homogeneous and orthotropic. The interfaces between the fiber and the matrix and between two adjacent plies are assumed to be perfectly bonded. A remote tensile stress σ_0 is applied in the longitudinal direction. The transverse matrix cracks are identical and equally spaced at $2L$ in the 90° plies and are of length $2a$. The crack density, number of cracks per unit length along the longitudinal direction, is defined as $\Gamma = 1/(2L)$. The thickness of the 90° ply group is denoted by $2w$. Unlike in the previous analytical models [1, 10, 20, 25–29], the crack length can be less than the thickness of the 90° ply group.

The cracked laminate is taken to be infinitely long in the longitudinal direction so that the mid-plane between any two consecutive cracks is a plane of symmetry and the longitudinal displacement on this mid-plane is uniform. With the above assumption, the problem shown in Fig. 1 can be idealized to the one in which a fixed displacement V_0 is applied on the ends of a sub-laminate in the longitudinal direction as shown in Fig. 2a. The fixed displacement V_0 can be related to the applied stress σ_0 by

$$V_0 = L\left(\frac{\sigma_0}{E_c} + \alpha_c \Delta T\right), \tag{1}$$

where E_c and α_c are the effective axial modulus and the effective axial coefficient of thermal expansion of the cracked laminate, respectively, and ΔT is the temperature change from stress free to service. A rectangular coordinate system is set up, with the x-axis coinciding with the crack plane and the y-axis coinciding with the orientation of the 0° plies, as shown in Fig. 2a. Further, due to symmetry of the sub-laminate

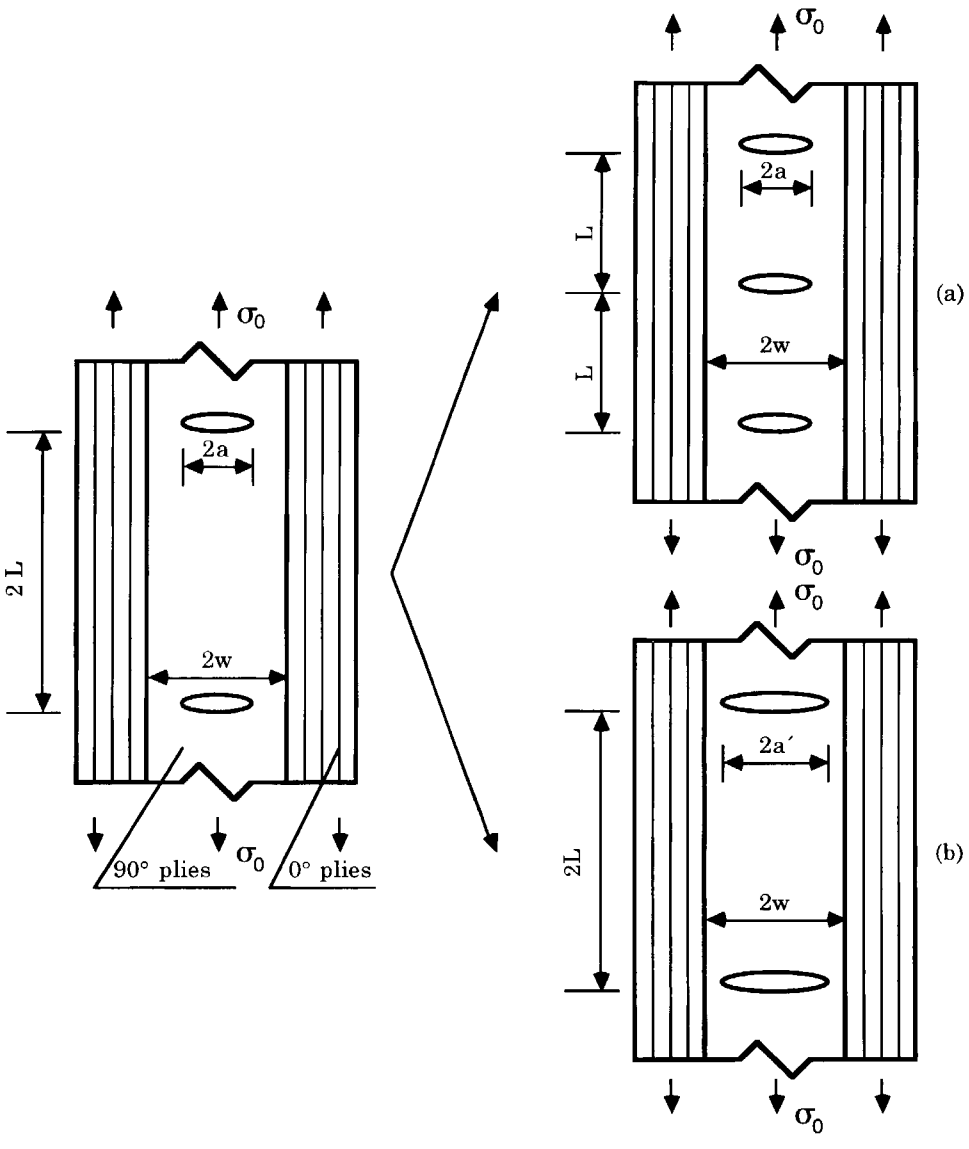

Figure 1. Evolution of microcracks in 90° plies in $[0_m^\circ/90_n^\circ]_s$ laminates subjected to tensile loading: (a) formation of new microcracks; (b) extension of pre-existing microcracks.

with respect to both x-axis and y-axis, only one quarter of the sub-laminate need be considered in the analysis. The sub-laminate is divided into several strips (elements) in order to carry out the numerical analysis. Note that no element spans two adjoining plies so that each element is homogenous and has a set of orthotropic material properties that correspond to the ply group in which the element is situated. A typical arrangement of these longitudinal elements is shown in Fig. 2b, and the element is identified by index $i = 1, 2, \ldots, M$.

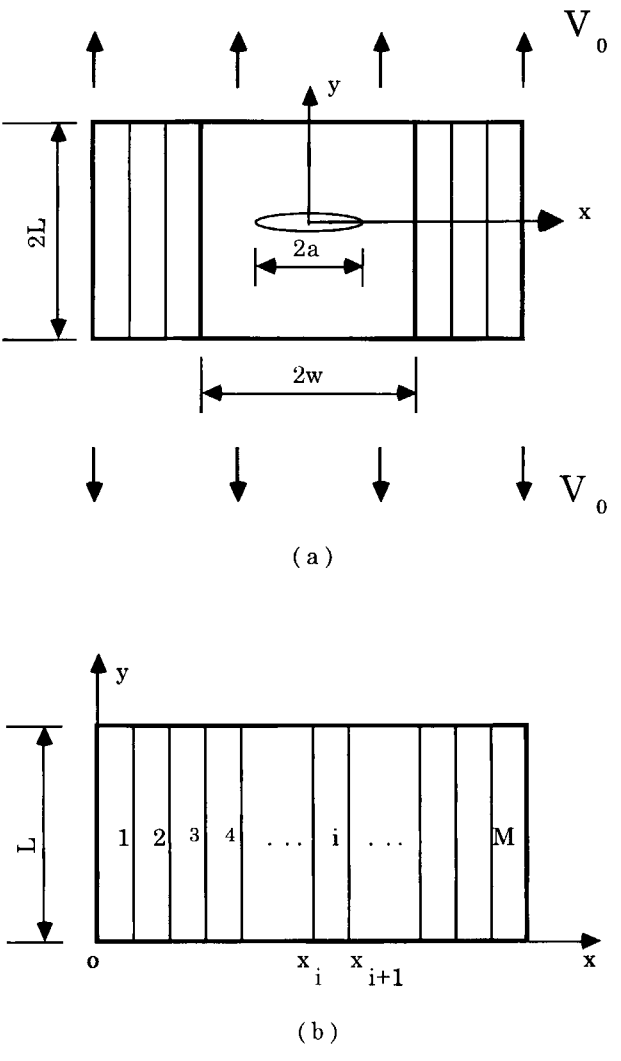

Figure 2. Equivalent sub-laminate showing the discretization scheme.

2.1. Total potential energy

For element i, let the displacements be $U_i(y)$ and $V_i(y)$ in the x- and y-directions, respectively. Using the finite-difference method, the strain-displacement relations for element i in the rectangular coordinate system can be approximated as follows:

$$\varepsilon_i^x = \frac{U_{i+1} - U_i}{x_{i+1} - x_i}, \tag{2}$$

$$\varepsilon_i^y = \frac{\mathrm{d}V_i}{\mathrm{d}y}, \tag{3}$$

$$\gamma_i^{xy} = \frac{dU_i}{dy} + \frac{V_{i+1} - V_i}{x_{i+1} - x_i}. \tag{4}$$

With reference to Fig. 2b, the orthotropic stress–strain relations for element i can be written as

$$\sigma_i^x = C_i^{xx}\left(\varepsilon_i^x - \alpha_i^x \Delta T\right) + C_i^{xy}\left(\varepsilon_i^y - \alpha_i^y \Delta T\right), \tag{5}$$

$$\sigma_i^y = C_i^{xy}\left(\varepsilon_i^x - \alpha_i^x \Delta T\right) + C_i^{yy}\left(\varepsilon_i^y - \alpha_i^y \Delta T\right), \tag{6}$$

$$\tau_i^{xy} = C_i^g \gamma_i^{xy}, \tag{7}$$

where C_i^{xx}, C_i^{xy}, C_i^{yy} and C_i^g are the orthotropic elastic constants for element i, and α_i^x and α_i^y are the thermal expansion coefficients in the x- and y-directions, respectively. These constants can be expressed in terms of the engineering constants of the lamina in which the element i is located and are listed in Appendix.

For this problem (Fig. 2b), the displacement boundary conditions are

$$V_i(L) = V_0 \quad \text{for all elements,} \tag{8}$$

$$V_i(0) = 0 \quad \text{for elements without crack,} \tag{9}$$

and the non-trivial force boundary condition does not manifest itself. The trival force boundary condition is not required in the numerical analysis based on the principle of minimum potential energy [32].

Based on the strain–stress relations, equations (5)–(7), we can express the strain energy U in the following form,

$$\begin{aligned} U = \frac{1}{2}\sum_{i=1}^{M}\int_0^L \Big[& C_i^{xx}\left(\varepsilon_i^x\right)^2 + C_i^{yy}\left(\varepsilon_i^y\right)^2 + 2C_i^{xy}\varepsilon_i^x\varepsilon_i^y + C_i^g\left(\gamma_i^{xy}\right)^2 \\ & - 2\left(C_i^{xx}\alpha_i^x + C_i^{xy}\alpha_i^y\right)\Delta T\,\varepsilon_i^x \\ & - 2\left(C_i^{xy}\alpha_i^x + C_i^{yy}\alpha_i^y\right)\Delta T\,\varepsilon_i^y \Big](x_{i+1} - x_i)h\,dy, \end{aligned} \tag{10}$$

where h is the width of the sub-laminate (in the z-direction) and will be taken as unity.

In the absence of the non-trivial force boundary condition, the potential energy is equal to the strain energy. After substitution of equations (2)–(4) into the above equation, the potential energy π_p can be obtained in terms of the displacement components as

$$\pi_p = U = \frac{1}{2}\sum_{i=1}^{M}\int_0^L (x_{i+1}-x_i)\left[C_i^{xx}\left(\frac{U_{i+1}-U_i}{x_{i+1}-x_i}\right)^2 + C_i^{yy}\left(\frac{dV_i}{dy}\right)^2\right.$$

$$+ 2C_i^{xy}\frac{U_{i+1}-U_i}{x_{i+1}-x_i}\frac{dV_i}{dy} + C_i^{g}\left(\frac{V_{i+1}-V_i}{x_{i+1}-x_i} + \frac{dU_i}{dy}\right)^2$$

$$- 2\left(C_i^{xx}\alpha_i^x + C_i^{xy}\alpha_i^y\right)\Delta T\frac{U_{i+1}-U_i}{x_{i+1}-x_i}$$

$$\left. - 2\left(C_i^{xy}\alpha_i^x + C_i^{yy}\alpha_i^y\right)\Delta T\frac{dV_i}{dy}\right] dy. \tag{11}$$

The principle of minimum potential energy (PMPE) for a sub-laminate subjected to a fixed displacement in the longitudinal direction on the ends may be expressed as

$$\delta\pi_p\left[U_i(y), V_i(y)\right] = 0, \tag{12}$$

along with equations (8) and (9). However, by employing the Lagrange multiplier method, which has wide applications in the variational methods in elasticity and plasticity [32], the PMPE can be modified as

$$\delta\pi_p^*\left[U_i(y), V_i(y), \lambda_i, \lambda_i^\circ\right] = \delta\left[\pi + \lambda_i V_i(L) + \lambda_i^\circ V_i(0)\right] = 0, \tag{13}$$

where λ_i and λ_i° are the Lagrange multipliers, and λ_i° is zero for the cracked elements. This form will be referred to as the modified principle of minimum potential energy (MPMPE). The constrained displacement boundary conditions which appear in the PMPE are not generally included in the MPMPE. This means that some of the problems with the displacement boundary conditions that are not easily amenable for solution using the PMPE could be solved by employing the MPMPE.

2.2. Numerical solution

Using the PMPE or the MPMPE, an approximate computation of displacements and stresses can be carried out. The procedure consists of first selecting the displacement functions containing some unknown parameters and, then, determining these unknown parameters by requiring the corresponding potential energy π_p or π_p^* to be a minimum. The displacement boundary conditions are required to be satisfied *a priori* for the PMPE, while this is not required for the MPMPE. In general, if the chosen displacement functions easily satisfy the displacement boundary conditions, the PMPE will be employed; otherwise, the modified PMPE will be employed.

We introduce the following set of power series for the displacement functions

$$U_i(y) = \sum_{s=0}^{T} A_i^s \left(\frac{y}{L}\right)^s, \tag{14}$$

$$V_i(y) = \sum_{s=0}^{T} B_i^s \left(\frac{y}{L}\right)^s, \tag{15}$$

where T is the order of a power series, and A_i^s and B_i^s are the unknown parameters yet to be determined. Substituting equations (14) and (15) into the energy equation (11), completing the integral, performing the variation and then using the MPMPE, equation (13), a system of linear algebraic equations can be obtained. Since the coefficient matrix of this system of linear algebraic equations is symmetric, only one-half of this system needs to be written as shown.

$$\sum_{s=0}^{T} \left\{ -\frac{LC_{i-1}^{xx}}{(1+s+s')(x_i - x_{i-1})} A_{i-1}^s + \left[\frac{L\left(C_{i-1}^{xx} + C_i^{xx}\right)}{(1+s+s')(x_i - x_{i-1})} + \frac{ss'C_i^g(x_{i+1} - x_i)}{(s+s'-1)L} \right] A_i^s + \frac{sC_{i-1}^{xy}}{(s+s')} B_{i-1}^s + \cdots \right\}$$
$$= \frac{L\left[\left(C_{i-1}^{xx}\alpha_{i-1}^x + C_{i-1}^{xy}\alpha_{i-1}^y\right) - \left(C_{i-1}^{xx}\alpha_{i-1}^x + C_{i-1}^{xy}\alpha_{i-1}^y\right)\right]\Delta T}{(1+s')}, \tag{16}$$

$$\sum_{s=0}^{T} \left\{ -\frac{sC_{i-1}^g}{s+s'} A_{i-1}^s + \left[-\frac{C_i^g s}{s+s'} - \frac{C_i^{xy} s'}{s+s'} \right] A_i^s - \frac{LC_{i-1}^g}{(s+s'+1)(x_i - x_{i-1})} B_{i-1}^s + \left[\frac{C_i^{xy} ss'(x_{i+1} - x_i)}{L(s+s'+1)} + \frac{LC_{i-1}^g}{(s+s'+1)(x_i - x_{i-1})} + \frac{LC_i^g}{(s+s'+1)(x_{i+1} - x_i)} \right] B_i^s + \cdots \right\} = (x_{i+1} - x_i)\left(C_i^{xy}\alpha_i^x + C_i^{yy}\alpha_i^y\right)\Delta T, \tag{17}$$

$$\sum_{s=0}^{T} B_i^s = V_0 \quad \text{for all elements,} \tag{18}$$

$$B_i^0 = 0 \quad \text{for uncracked elements,} \tag{19}$$

where s' and i vary from 0 to T and 1 to M, respectively.

Once this system of governing equations for the unknown parameters A_i^s, B_i^s, λ_i and λ_i° are solved, the complete displacement and stress distributions can be determined. The corresponding strain energy can be calculated by using equation (11), which will be applied to the failure analysis of transverse cracking.

Recalling equation (1), the effective axial modulus and the effective axial coefficient of thermal expansion of the cracked laminates can be given as follows,

$$E_c = \frac{L(\sigma_{01} - \sigma_{02})}{V_{01} - V_{02}}, \tag{20}$$

$$\alpha_c = \frac{\sigma_{01} V_{02} - \sigma_{02} V_{01}}{(\sigma_{01} - \sigma_{02}) L \Delta T}, \tag{21}$$

where V_{01} and V_{02} are the distinct applied displacements on the ends of sub-laminates, and σ_{01} and σ_{02} are the axial stresses on the ends corresponding to the applied displacements V_{01} and V_{02}, respectively.

Since the thermal effect is included in the analysis, the strain energy U varies as a parabolic function of the applied displacement V_0 as follows:

$$U = U_a + U_b V_0 + U_c V_0^2. \tag{22}$$

The coefficients U_a, U_b and U_c are independent of the applied displacement V_0, but depend on the crack configuration of the sub-laminates, the material properties and the thermal effect. They can be determined by the following equations:

$$\begin{aligned} U_a = {} & \big(U_1 V_{02} V_{03}^2 + U_2 V_{03} V_{01}^2 + U_3 V_{01} V_{02}^2 - U_3 V_{02} V_{01}^2 \\ & - U_1 V_{03} V_{02}^2 - U_2 V_{01} V_{03}^2\big) \\ & / \big(V_{02} V_{03}^2 + V_{01} V_{02}^2 + V_{03} V_{01}^2 - V_{02} V_{01}^2 - V_{03} V_{02}^2 - V_{01} V_{03}^2\big), \end{aligned} \tag{23}$$

$$\begin{aligned} U_b = {} & \big(U_1 V_{02}^2 + U_2 V_{03}^2 + U_3 V_{01}^2 - U_1 V_{03}^2 - U_2 V_{01}^2 - U_3 V_{02}^2\big) \\ & / \big(V_{02} V_{03}^2 + V_{01} V_{02}^2 + V_{03} V_{01}^2 - V_{02} V_{01}^2 - V_{03} V_{02}^2 - V_{01} V_{03}^2\big), \end{aligned} \tag{24}$$

$$\begin{aligned} U_c = {} & \big(U_1 V_{03} + U_2 V_{01} + U_3 V_{02} - U_1 V_{02} - U_2 V_{03} - U_3 V_{01}\big) \\ & / \big(V_{02} V_{03}^2 + V_{01} V_{02}^2 + V_{03} V_{01}^2 - V_{02} V_{01}^2 - V_{03} V_{02}^2 - V_{01} V_{03}^2\big), \end{aligned} \tag{25}$$

where V_{01}, V_{02} and V_{03} are three distinct values of the applied displacement, and U_1, U_2 and U_3 are the corresponding values of the strain energy of the sub-laminates, respectively, which are calculated by using equation (11).

The strain energy of the cracked composite laminate per unit length can be expressed in terms of

$$U_{\text{total}} = \Gamma U = \Gamma\left(U_a + U_b V_0 + U_c V_0^2\right) = \Gamma U_a + U_b V_{\text{total}} + \frac{U_c V_{\text{total}}^2}{\Gamma}, \tag{26}$$

where $V_{\text{total}} = V_0\Gamma$ is the total applied displacement on the cracked laminate.

2.3. *Fracture analysis*

The strain energy release rate G is given by

$$G = -\left.\frac{\partial U_{\text{total}}}{\partial A}\right|_{V_{\text{total}}}, \tag{27}$$

where A is the total area of crack and V_{total} is the total applied displacement.

As mentioned earlier, two failure modes are considered in this paper: one is the formation of a new transverse crack and the other is the extension of pre-existing cracks (Fig. 1). First, the strain energy release rate for the formation of a new crack is derived. Since the axial stress σ_y is maximum on the midplane between two adjacent cracks, a new crack is likely to form on this plane. After the formation of new cracks, the crack density will double to 2Γ. From equation (26), the change in the total strain energy U_{total} due to the formation of new cracks can be obtained as

$$\begin{aligned}\Delta U_{\text{total}} = {} & U_{\text{total}}\left(2\Gamma, \frac{a}{w}\right) - U_{\text{total}}\left(\Gamma, \frac{a}{w}\right) = 2\Gamma U_a\left(2\Gamma, \frac{a}{w}\right) - \Gamma U_a\left(\Gamma, \frac{a}{w}\right) \\ & + \left[U_b\left(2\Gamma, \frac{a}{w}\right) - U_b\left(\Gamma, \frac{a}{w}\right)\right] V_{\text{total}} \\ & + \left[U_c\left(2\Gamma, \frac{a}{w}\right) - 2U_c\left(\Gamma, \frac{a}{w}\right)\right] \frac{V_{\text{total}}^2}{2\Gamma},\end{aligned} \tag{28}$$

and the change in the crack area due to the formation of new cracks is given by

$$\Delta A = 4\Gamma a - 2\Gamma = 2\Gamma a. \tag{29}$$

Substituting equations (28) and (29) into equation (27), the strain energy release rate for new crack formation can be obtained as,

$$G_{\text{new}} = -\frac{2U_a\left(2\Gamma, \frac{a}{w}\right) - U_a\left(\Gamma, \frac{a}{w}\right)}{2a} - \frac{\left[U_b\left(2\Gamma, \frac{a}{w}\right) - U_b\left(\Gamma, \frac{a}{w}\right)\right]V_{\text{total}}}{2\Gamma a} - \frac{\left[U_c\left(2\Gamma, \frac{a}{w}\right) - 2U_c\left(\Gamma, \frac{a}{w}\right)\right]V_{\text{total}}^2}{4\Gamma^2 a}. \tag{30}$$

Similarly, using equations (26) and (27), the strain energy release rate for the extension of pre-existing cracks is given by

$$G_{\text{ex}} = -\frac{1}{2}\frac{\partial U_a\left(\Gamma, \frac{a}{w}\right)}{\partial a} - \frac{V_{\text{total}}}{2\Gamma}\frac{\partial U_b\left(\Gamma, \frac{a}{w}\right)}{\partial a} - \frac{V_{\text{total}}^2}{2\Gamma^2}\frac{\partial U_c\left(\Gamma, \frac{a}{w}\right)}{\partial a}. \tag{31}$$

If the strain energy release rate is employed, the critical applied displacements for two failure modes, V_{cnew} and V_{cex} can be calculated by

$$G_{\text{new}}(V_{\text{cnew}}) = G_{\text{c}}, \tag{32}$$

$$G_{\text{ex}}(V_{\text{cex}}) = G_{\text{c}}, \tag{33}$$

where G_{c} is the fracture toughness of lamina in transverse direction.

Using equation (1), the critical applied displacement V_{cnew} and V_{cex} can be converted to the critical applied stresses for the formation of new cracks and the extension of a pre-existing crack, σ_{cn} and σ_{ce}, as follows,

$$\sigma_{\text{cn}} = (2V_{\text{cnew}} - \alpha_{\text{c}}\Delta T)E_{\text{c}}, \tag{34}$$

$$\sigma_{\text{ce}} = (2V_{\text{cex}} - \alpha_{\text{c}}\Delta T)E_{\text{c}}. \tag{35}$$

By comparing the magnitude of σ_{cn} with that of σ_{ce}, the mode of failure can be determined. If $\sigma_{\text{cn}} < \sigma_{\text{ce}}$, new cracks will be formed while if $\sigma_{\text{cn}} > \sigma_{\text{ce}}$ the crack will extend in a self-similar fashion.

3. RESULTS AND DISCUSSION

A computer code has been developed to solve the system of governing linear algebraic equations (16)–(19) for A_i^s, B_i^s, λ_i and λ_i°, and then to compute the strain energy, effective axial modulus and effective axial thermal expansion coefficient for different crack and laminate configurations. The critical applied stresses σ_{cn} and σ_{ce} can be obtained, if the fracture toughness G_c is known. A uniform mesh with 60 elements for each lamina is employed in the numerical computation. The order of power polynomials (T) in equations (14) and (15) is taken to be 9 for all cases for a satisfactory convergence of the numerical solution. In the parametric studies, two systems of composite materials, glass/epoxy and ceramic/ceramic (SiC/1723) are considered. The material properties used in the model predictions are given in Table 1.

Figures 3 and 4 show the effective axial modulus of the laminate as a function of the crack density for a fixed crack length in a $[0_3^\circ/90^\circ]_s$ SiC/1723 and a $[0_3^\circ/90^\circ]_s$ glass/epoxy laminate, respectively. The effective axial modulus is dependent on the crack density as well as the crack length; an increase in both crack density and crack length leads to a reduction in the effective axial modulus, as expected. The variation of the effective axial coefficient of thermal expansion due to transverse cracking is investigated and presented next. Figures 5 and 6 show the effective axial coefficient of thermal expansion as a function of the crack density for a fixed crack length for a $[0_3^\circ/90^\circ]_s$ SiC/1723 and a $[0^\circ/90_3^\circ]_s$ glass/epoxy laminate, respectively. The change in the effective axial coefficient of thermal expansion due to transverse cracking is much more significant in the case of SiC/1723 laminates than that of glass/epoxy laminates. For a special case with the $\Gamma = 1.0$ and $a/w = 1.0$, the value of α_c decreases from $15.20 \times 10^{-6}/^\circ C$ to $10.3 \times 10^{-6}/^\circ C$ for the $[0^\circ/90_3^\circ]_s$ glass/epoxy laminate as compared to $3.65 \times 10^{-6}/^\circ C$ to $3.55 \times 10^{-6}/^\circ C$ for the SiC/1723 laminate.

The variation of the critical stress for new crack formulation as a function of the crack density for the various values of the crack length for a $[0_3^\circ/90^\circ]_s$ SiC/1723 composite laminate is plotted in Fig. 7. The critical stress for new crack formation increases as the crack density increases, implying that the formation of new cracks

Table 1.
Material properties used in the model predictions

Property	SiC/1723	Glass/epoxy
E_1 (GPa)	140	42
$E_2 = E_3$ (GPa)	88	13
$\nu_{12} = \nu_{13}$	0.20	0.30
ν_{23}	0.26	0.42
$G_{12} = G_{13}$ (GPa)	44.0	3.4
G_{23} (GPa)	35.0	4.57
G_c (J/m^2)	9.0	330.0
α_1 ($10^{-6}/^\circ C$)	3.54	8.10
α_2 ($10^{-6}/^\circ C$)	3.92	22.10
ΔT (°C)	−500.0	−150.0
Lamina thickness (mm)	0.242	0.203

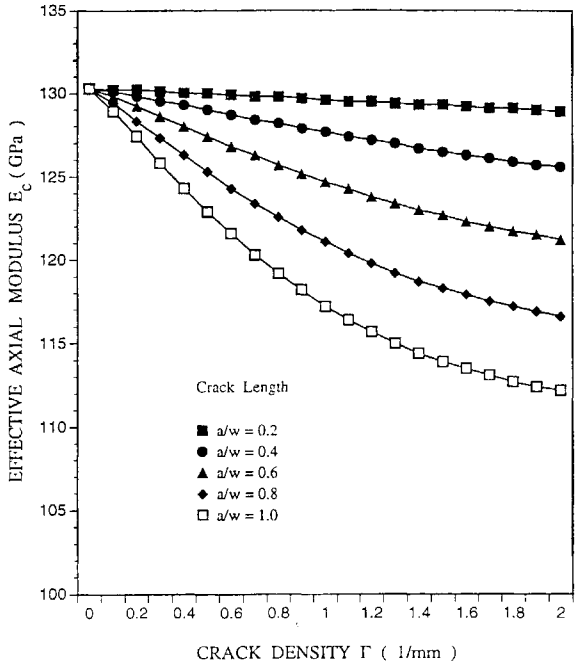

Figure 3. Effective axial modulus as a function of crack density for a fixed crack length for a $[0_3^\circ/90^\circ]_s$ SiC/1723 laminate.

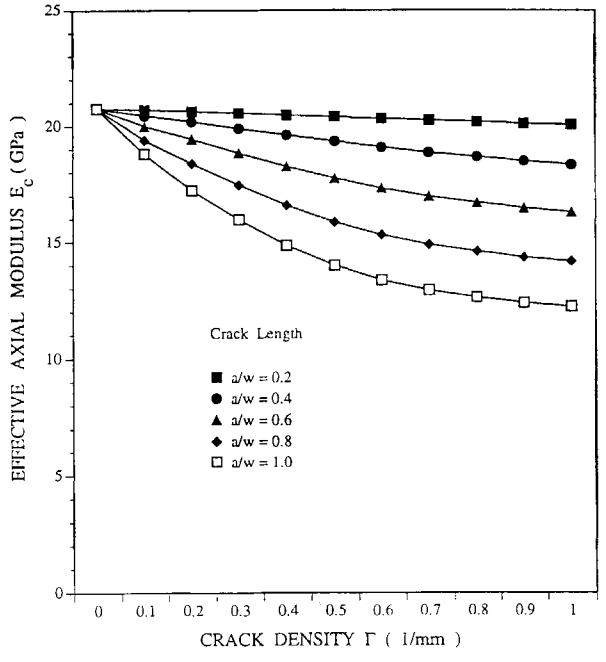

Figure 4. Effective axial modulus as a function of crack density for a fixed crack length for a $[0^\circ/90_3^\circ]_s$ glass/epoxy laminate.

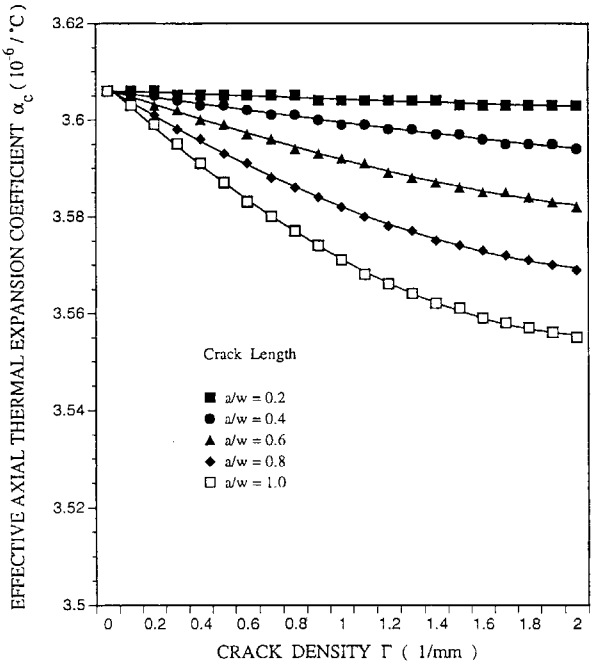

Figure 5. Effective axial coefficient of thermal expansion as a function of crack density for a fixed crack length for a $[0_3^\circ/90^\circ]_s$ SiC/1723 laminate.

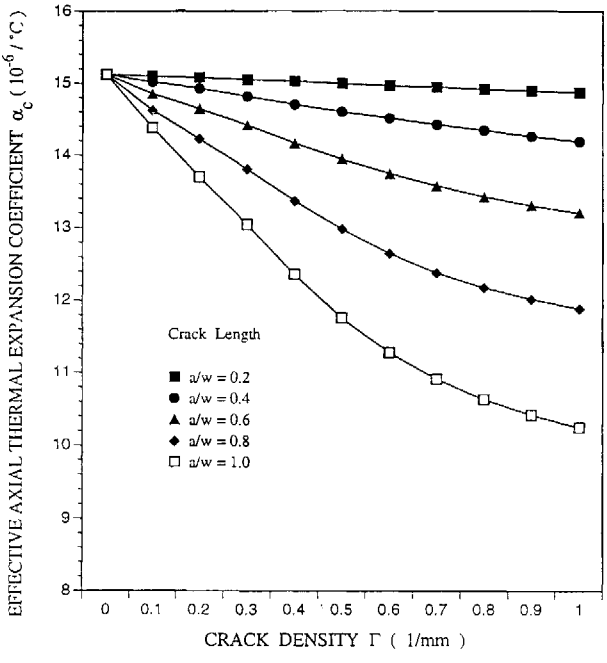

Figure 6. Effective axial coefficient of thermal expansion as a function of crack density for a fixed crack length for a $[0^\circ/90_3^\circ]_s$ glass/epoxy laminate.

becomes stable with the increasing applied load. However, the effect of the crack length on the critical stress for new crack formation is more complicated. When the crack density is less than 1.0/mm, larger critical stresses for new crack formation correspond to a smaller crack length. When the crack density is more than 1.0/mm, the situation is opposite. When the crack density Γ is approximately 1.0/mm, the critical stress for new crack formation is almost independent of the crack length, and this will be referred to as transition crack density Γ_t. The results corresponding to crack length $a/w = 0.2$, however, do not follow the same trend. A possible explanation is that the crack length $a/w = 0.2$ belongs to small crack case and there is no interaction between adjacent cracks. Figure 8 shows the critical stress for new crack formation as a function of the crack density for different values of the crack length for a $[0°/90°_3]_s$ glass/epoxy laminate. The glass/epoxy laminate exhibits the same behavior as the SiC/1723 laminate. The difference is in the transition crack density $\Gamma_t = 0.65$/mm for the $[0°/90°_3]_s$ glass/epoxy laminate.

The critical stress for the extension of a pre-existing crack is calculated as a function of the crack density for various values of the crack length and plotted in Figs 9 and 10 for a $[0°_3/90°]_s$ SiC/1723 and a $[0°/90°_3]_s$ glass/epoxy laminate, respectively. For a given crack density, the critical stress for the extension of a pre-existing crack decreases as the crack length increases; the self-similar extension of a pre-existing crack is unstable. Once the applied stress reaches the critical stress for a certain crack configuration, pre-existing cracks will grow until they impinge on the 0°/90° interface. Also, for very low crack density, the critical stress for crack extension decreases with the crack density. For higher crack density, the critical stress for crack extension increases slightly with the increase in the crack density.

Comparing Fig. 7 with Fig. 9 and Fig. 8 with Fig. 10, we find that for any crack configurations, the value of the critical stress for crack extension is always less than that of the critical stress for the formation of new cracks. Therefore, the extension of the pre-existing cracks in 90° plies will take place first, once the applied stress reaches the corresponding critical stress and they will grow unstably until the crack tips reach the 0°/90° interface. Then, the formation of new cracks in 90° plies will begin.

In order to validate the results presented in this paper, a comparison between the model predictions and the available experimental data is presented in Figs 11 and 12 for a $[0°_3/90°]_s$ SiC/1723 laminate and a $[0°/90°_3]_s$ glass/epoxy laminate, respectively. Experimental data for both SiC/1723 and glass/epoxy laminates show that the crack density increases with an increase in applied stress and then a saturation state is reached at which point the cracks do not multiply with the increasing stress level. This characteristic saturation density for the SiC/1723 laminate is approximately 1.75 cracks/mm while the corresponding density for the glass/epoxy laminate is approximately 1.75 cracks/mm. The model predictions agree fairly well with the experimental data below the corresponding characteristic saturation densities. However, the model predictions do not show a saturation density; crack density continues to increase with the applied stress. In experiments it has been observed that, at the saturation density, extensive debonding at the 0°/90° interface takes place. The proposed model in the current form does not account for this change in the failure mode.

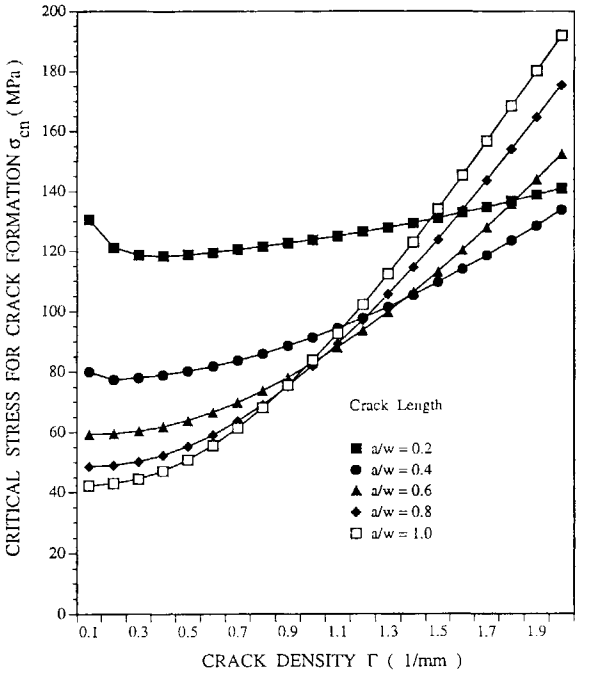

Figure 7. Critical stress for new crack formation as a function of crack density for different values of crack length for a $[0_3^\circ/90^\circ]_S$ SiC/1723 laminate.

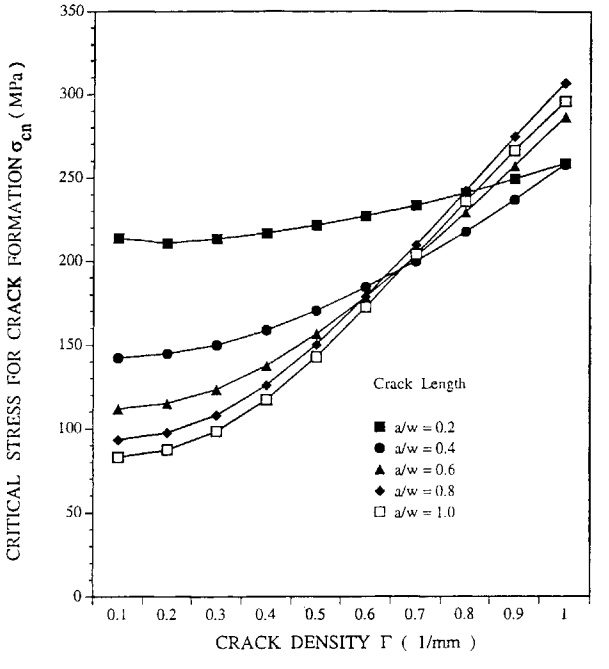

Figure 8. Critical stress for new crack formation as a function of crack density for different values of crack length for a $[0^\circ/90_3^\circ]_S$ glass/epoxy laminate.

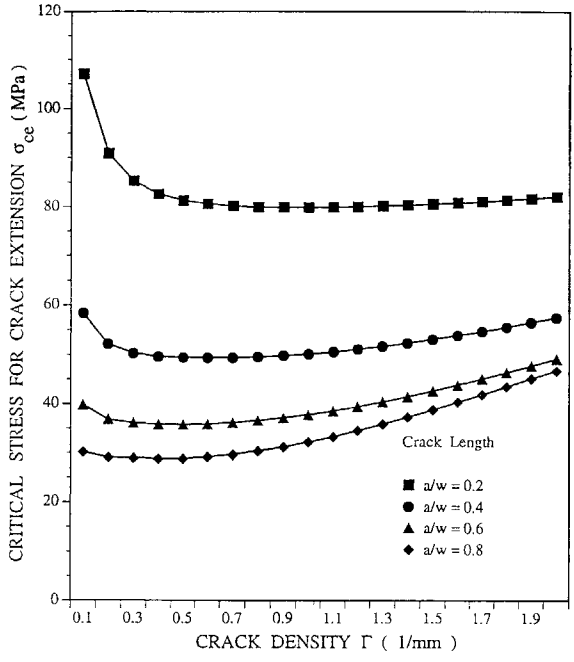

Figure 9. Critical stress for the extension of an existing crack as a function of crack density for different values of crack length for a $[0°/90°_3]_S$ SiC/1723 laminate.

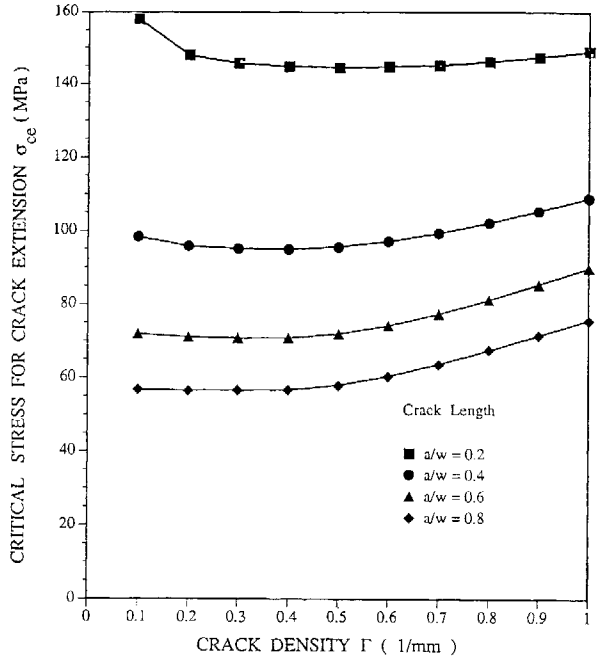

Figure 10. Critical stress for the extension of an existing crack as a function of crack density for different values of crack length for a $[0°_3/90°]_S$ glass/epoxy laminate.

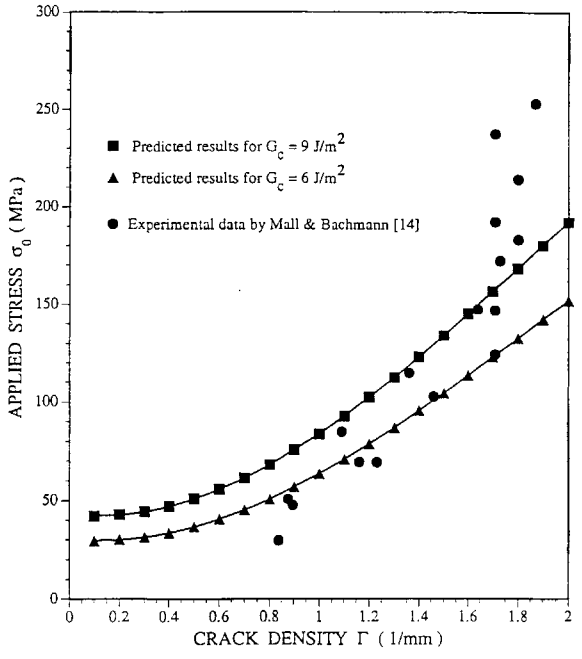

Figure 11. Comparison of analytical predicted results with the experimental data for a $[0_3^\circ/90^\circ]_s$ SiC/1723 laminate with transverse cracks of length $a/w = 1.0$.

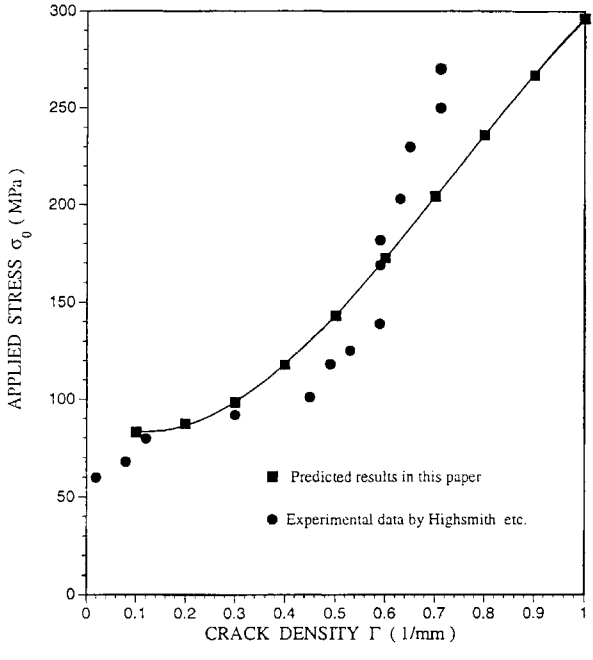

Figure 12. Comparison of analytical predicted results with the experimental data for a $[0^\circ/90_3^\circ]_s$ glass/epoxy laminate with transverse cracks of length $a/w = 1.0$.

The authors are planning to include the combined transverse cracking and interface debonding at the 0°/90° interface in their future investigations.

4. CONCLUSIONS

The analytical model developed in this paper based on the principle of minimum potential energy can be used to analyze the formation and the extension of transverse cracks in the 90° plies of $[0^\circ_m/90^\circ_n]_s$ composite laminates. By comparing the results presented in this paper with the available experimental data, it is found that the results predicted by the numerical approach are reliable, albeit in the early stages of damage evolution. By analyzing the computed results, it is found that the fracture process of cross-ply laminates containing transverse cracks in the 90° plies includes two stages: the first is the unstable extension of pre-existing cracks until the crack tips reach the 0°/90° interface, and the second is the stable formation of new cracks.

REFERENCES

1. Garrett, K. W. and Bailey, J. E. Multiple transverse fracture in 90° cross-ply laminates of a glass fiber-reinforced polyester. *J. Mater. Sci.* **12**, 157–168 (1977).
2. Parvizi, A., Garrett, K. W. and Bailey, J. E. Constrained cracking in glass fibre-reinforced epoxy cross-ply laminates. *J. Mater. Sci.* **13**, 195–201 (1978).
3. Bailey, J. E., Curtis, P. T. and Parvizi, A. On the transverse cracking and longitudinal splitting behavior of glass and carbon fibre reinforced epoxy cross-ply laminates and the effect of Poisson and thermally generated strain. *Proc. Roy. Soc. London A* **366**, 599–623 (1979).
4. Highsmith, A. L. and Reifsnider, K. L. Stiffness-reduction mechanisms in composite laminates. In: *Damage in Composite Materials, ASTM STP 775*, Reifsnider, K. L. (Ed.). Am. Soc. for Testing and Mater. (1982), pp. 103–117.
5. Crossman, F. W. and Wang, A. S. D. The dependence of transverse cracks and delamination on ply thickness in graphite-epoxy laminates. In: *Damage in Composite Materials, ASTM STP 775*, Reifsnider, K. L. (Ed.). Am. Soc. for Testing and Mater. (1982), pp. 118–139.
6. Wang, A. S. D., Chou, P. C., Lei, S. C. and Bucinell, R. B. Cumulative damage model for advanced composite materials, Phase-II. Final Report on Contract No. F33615-80-C-5039, Air Force Wright Aeronautical Laboratories, USA (1983).
7. Wang, A. S. D. Fracture mechanics of sublaminate cracks in composite materials. *Compos. Technol. Rev.* **6**, 45–62 (1984).
8. Ogin, S. L., Smith, P. A. and Beaumont, P. W. R. Matrix cracking and stiffness reduction during the fatigue of $[0^\circ/90^\circ]_s$ GFRP laminate. *Compos. Sci. Technol.* **22**, 23–31 (1985).
9. Smith, P. A. and Wood, J. R. Poisson's ratio as a damage parameter in the static tensile loading of simple crossply laminates. *Compos. Sci. Technol.* **38**, 85–93 (1990).
10. Liu, S. and Nairn, J. A. The formation and propagation of matrix microcracks in cross-ply laminates during static loading. *J. Reinf. Plastics Compos.* **11**, 158–178 (1992).
11. Dvorak, G. J. and Johnson, W. S. Fatigue of metal matrix composites. *Int. J. Fracture* **16**, 585–607 (1980).
12. Seerat-un-Nabi, A. and Derby, B. Mechanical properties of laminated pyrex matrix composites. In: *Proc. 9th Riso Int. Symp. on Met. & Mater. Sci.* Roskilde, Denmark (1988), pp. 463–468.
13. Pryce, A. W. and Smith, P. A. The behavior of unidirectional and crossply ceramic matrix composites under quasi-static tensile loading. *J. Mater. Sci.* **27**, 2695–2704 (1992).
14. Mall, S. and Bachmann, S. E. Transverse cracking in a fiber reinforced ceramic matrix composite. In: *Proc. Sixth Japan–US Conference on Composite Materials*. Orlando, FL (1992), pp. 262–270.

15. Laws, N. and Dvorak, G. J. The loss of stiffness of cracked laminates. In: *Proc. IUTAM Eshelby Memorial Symp.* Sheffield, England (1985), pp. 119–128.
16. Talreja, R. Transverse cracking and stiffness reduction in composite laminates. *J. Compos. Mater.* **19**, 355–375 (1985).
17. Hashin, Z. Analysis of stiffness reduction of cracked cross-ply laminates. *Engineering Fracture Mechanics* **25**, 771–778 (1986).
18. Aboudi, J. Stiffness reduction of cracked solids. *Engineering Fracture Mechanics* **26**, 637–650 (1987).
19. Nuismer, R. J. and Tan, S. C. Constitutive relations of a crack composite lamina. *J. Compos. Mater.* **22**, 306–321 (1988).
20. Han, Y. M. and Hahn, H. T. Ply cracking and property degradations of symmetric balanced laminates under general in-plane loading. *Compos. Sci. Technol.* **35**, 377–397 (1989).
21. Zhang, J., Fan, J. and Soutis, C. Analysis of multiple matrix cracking in $[\pm\theta_m/90_n^\circ]_s$ composite laminates, Part 1: In-plane stiffness properties. *Composites* **23**, 291–298 (1992).
22. Dharani, L. R. and Ji, F. S. Effect of transverse cracking on stiffness reduction of cross-ply laminates. *Appl. Compos. Mater.* **2**, 217–231 (1995).
23. Herakovich, C. T. and Hyer, M. W. Damage-induced property changes in composites subjected to cyclic thermal loading. *Engineering Fracture Mechanics* **25**, 779–791 (1986).
24. Hashin, Z. Thermal expansion coefficient of cracked laminates. *Compos. Sci. Technol.* **31**, 247–260 (1988).
25. Nairn, J. A. The strain energy release rate of composite microcracking: a variational approach. *J. Compos. Mater.* **23**, 1106–1129 (1989).
26. Flaggs, D. L. Prediction of tensile matrix failure in composite laminates. *J. Compos. Mater.* **19**, 29–50 (1985).
27. Wang, A. S. D., Chou, P. C. and Lei, S. C. A stochastic model for the growth of matrix cracks in composite laminates. *J. Compos. Mater.* **18**, 239–254 (1984).
28. Laws, N. and Dvorak, G. J. Progressive transverse cracking in composite laminates. *J. Compos. Mater.* **22**, 900–916 (1988).
29. Zhang, J., Fan, J. and Soutis, C. Analysis of multiple matrix cracking in $[\pm\theta_m/90_n^\circ]_s$ composite laminates, Part 2: Development of transverse ply cracks. *Composites* **23**, 299–304 (1992).
30. Guild, F. J., Ogin, S. L. and Smith, P. A. Modelling of 90° ply cracking in cross-ply laminates, including three-dimensional effects. *J. Compos. Mater.* **27**, 646–667 (1993).
31. Zhao, J. H. and Ji, F. S. Stress analysis of unidirectional composites with a surface notch by variational principle. *Engineering Fracture Mechanics* **37**, 727–733 (1990).
32. Washizu, K. *Variational Methods in Elasticity and Plasticity*, 3rd edn. Pergamon Press, Oxford, England (1982).

APPENDIX

If element i is located in the 90° plies, the elastic constants C_i^{xx}, C_i^{xy}, C_i^{yy} and C_i^g, can be written in terms of

$$C_i^{xx} = \frac{1 - \nu_{12}\nu_{21}}{E_1 E_2 \Delta},$$

$$C_i^{xy} = \frac{\nu_{32} + \nu_{12}\nu_{31}}{E_1 E_3 \Delta},$$

$$C_i^{yy} = \frac{1 - \nu_{31}\nu_{13}}{E_1 E_3 \Delta},$$

$$C_i^g = G_{23},$$

and if element i is located in the zero plies, the elastic constants can be given as follows

$$C_i^{xx} = \frac{1 - \nu_{13}\nu_{31}}{E_1 E_3 \Delta},$$
$$C_i^{xy} = \frac{\nu_{21} + \nu_{31}\nu_{23}}{E_2 E_3 \Delta},$$
$$C_i^{yy} = \frac{1 - \nu_{23}\nu_{32}}{E_2 E_3 \Delta},$$
$$C_i^{g} = G_{12},$$

where

$$\nu_{21} = \frac{\nu_{12} E_2}{E_1},$$
$$\nu_{31} = \frac{\nu_{13} E_3}{E_1},$$
$$\nu_{32} = \frac{\nu_{23} E_3}{E_2},$$
$$\Delta = \frac{1 - \nu_{12}\nu_{21} - \nu_{23}\nu_{32} - \nu_{13}\nu_{31} - 2\nu_{21}\nu_{32}\nu_{13}}{E_1 E_2 E_3}.$$

If element i is located in the 90° plies, the thermal expansion coefficients α_i^x and α_i^y can be expressed as

$$\alpha_i^x = \alpha_2,$$
$$\alpha_i^y = \alpha_2,$$

and if element i is located in the 0° plies, the thermal expansion coefficients α_i^x and α_i^y can be written as

$$\alpha_i^x = \alpha_2,$$
$$\alpha_i^y = \alpha_1.$$